nature physics

Article https://doi.org/10.1038/s41567-024-02407-1

Graph states of atomic ensembles engineered by photon-mediated entanglement

In the format provided by the authors and unedited

Engineering Graph States of Atomic Ensembles by Photon-Mediated Entanglement: Supplementary Information

This supplement provides supporting derivations pertaining to the spin-nematic squeezing dynamics and the verification of entanglement, as well as supporting measurements. Section I presents matrix representations of spin-1 operators and motivates the generalized Bloch sphere for visualization of the spin-1 dynamics. Section II presents a derivation of the metrological squeezing parameter for spin-f atoms. Section III provides an alternative determination of the contrast used in calculating normalized variances and metrological squeezing. In Sec. IV we analytically derive the initial dynamics of spin-nematic squeezing and discuss both technical and fundamental limits on the achievable multimode squeezing.

I. SPIN-1 ALGEBRA AND GENERALIZED BLOCH SPHERE

The matrix forms of the spin-1 dipole operators are

$$f^x = \frac{1}{\sqrt{2}} \begin{pmatrix} 0 & 1 & 0 \\ 1 & 0 & 1 \\ 0 & 1 & 0 \end{pmatrix}, \; f^y = \frac{1}{\sqrt{2}} \begin{pmatrix} 0 & -i & 0 \\ i & 0 & -i \\ 0 & i & 0 \end{pmatrix}, \; f^z = \begin{pmatrix} 1 & 0 & 0 \\ 0 & 0 & 0 \\ 0 & 0 & -1 \end{pmatrix}. \tag{S1}$$

From these matrices and the definitions in Methods Sec. A, we can also readily construct the matrix representations of the quadrupole operators $q^{\alpha\beta} = f^\alpha f^\beta + f^\beta f^\alpha - \frac{4}{3} I_3 \delta_{\alpha\beta}$ and $q^0 = q^{zz} + \frac{1}{3} I_3$, where I_3 is the identity matrix and $\delta_{\alpha\beta}$ is the Kronecker delta function. For example,

$$q^{zz} = \begin{pmatrix} 2/3 & 0 & 0 \\ 0 & -4/3 & 0 \\ 0 & 0 & 2/3 \end{pmatrix}, \; q^0 = \begin{pmatrix} 1 & 0 & 0 \\ 0 & -1 & 0 \\ 0 & 0 & 1 \end{pmatrix}, \; q^{yz} = \frac{i}{\sqrt{2}} \begin{pmatrix} 0 & -1 & 0 \\ 1 & 0 & 1 \\ 0 & -1 & 0 \end{pmatrix}. \tag{S2}$$

We visualize the spin-1 dynamics in an approximate SU(2) subspace spanned by F^x, Q^{yz}, and Q^0, where $F^\alpha = \sum_i^N f_i^\alpha$ and $Q^{\alpha\beta} = \sum_i^N q_i^{\alpha\beta}$ denote collective observables for the system of N atoms. This visualization is motivated by the commutation relations

$$\begin{aligned} [Q^{yz}, Q^0] &= 2iF^x \\ [Q^0, F^x] &= 2iQ^{yz} \\ [F^x, Q^{yz}] &= i(Q^{zz} - Q^{yy}) = 2i(Q^0 - D), \end{aligned} \tag{S3}$$

where $D = (Q^{zz} + Q^{yy} - Q^{xx})/4 + N/3$ commutes with F^x, Q^{yz}, and Q^0. For a Larmor-invariant system with only a small side-mode population, $\langle D \rangle = (N_{+1} + N_{-1})/2 \ll \langle Q^0 \rangle$. This justifies the use of Q^0, which is directly accessible from the atomic populations N_m, for the purpose of visualization on the generalized Bloch sphere in Figures 1b and S1a. While these figures show the $\{F^x, Q^{yz}, Q^0\}$ sphere, identical dynamics occur in the approximate SU(2) subspace spanned by F^y, Q^{xz}, and Q^0, as our system is Larmor invariant.

II. ENTANGLEMENT DETECTION VIA METROLOGICAL GAIN

Squeezing within a single mode can be used to directly witness entanglement when the generated states circumvent limits on the metrological sensitivity of unentangled states. The appropriate measure of squeezing for this context is the Wineland parameter ξ^2 defined in the main text, which quantifies enhanced sensitivity to rotations [1, 2] — in our case on the quadrupole spin sphere with axes $\{F^x, Q^{yz}, Q^0\}$. Entanglement is necessary for reaching values of this metrological squeezing parameter that are below the standard quantum limit (SQL) $\xi^2 = 1$.

As the seminal work defining the Wineland squeezing parameter focused on ensembles of spin-1/2 particles [1], we show here how the connection between metrological gain and entanglement generalizes to systems with larger internal spin f, including the spin-1 atoms in this work [3]. Generically, the derivation of a Wineland criterion for entanglement follows from considering the metrological task of estimating a parameter λ in a unitary transformation of the form $U = e^{i\lambda\mathcal{H}}$. To derive a criterion suitable for detecting spin-nematic squeezing, we assume without loss of generality that the squeezed quadrature is F^x and consider the resulting enhancement in sensitivity to rotations generated by $\mathcal{H} = Q^{yz}$.

We first derive the standard quantum limit on the sensitivity attainable to rotations about Q^{yz} using an unentangled state of N atoms. For any initial state specified by a density matrix ρ, the quantum Cramer-Rao bound limits the precision of estimating the angle λ in a single trial to

$$\Delta\lambda \geq \frac{1}{\sqrt{\mathcal{F}[\rho, \mathcal{H}]}}, \tag{S4}$$

where

$$\mathcal{F}[\rho, \mathcal{H}] \leq 4\mathrm{Var}\left(\mathcal{H}\right)_\rho \tag{S5}$$

is the quantum Fisher information [4, 5], and the inequality in Eq. (S5) is saturated by pure states. For product states, the quantum Fisher information for detecting rotations about Q^{yz} is limited to

$$F_Q[\rho, Q^{yz}] \leq 4\mathrm{Var}\left(Q^{yz}\right)_\rho = 4\sum_i \mathrm{Var}\left(q_i^{yz}\right)_\rho \leq 4Nf^2, \tag{S6}$$

where in the last inequality the single-atom spin $f = 1$ dictates that $\mathrm{Var}\left(q_i^{yz}\right) \leq f^2$. Thus, the minimum imprecision of a measurement of λ using an unentangled state is $\Delta\lambda_{\mathrm{SQL}} = 1/(2f\sqrt{N})$.

The Wineland parameter compares the sensitivity of an arbitrary state to the standard quantum limit. Assuming that the state is used to estimate λ via the dependence of $\langle F^x\rangle$ on the rotation about Q^{yz}, the uncertainty $\Delta\lambda$ is related to the spin variance $\mathrm{Var}\left(F^x\right)$ by

$$(\Delta\lambda)^2 = \frac{\mathrm{Var}\left(F^x\right)}{\left(d\left\langle F^x\right\rangle/d\lambda\right)^2}, \tag{S7}$$

where the rate of change $d\left\langle F^x\right\rangle/d\lambda$ of $\langle F^x\rangle$ under the Hamiltonian $\mathcal{H} = Q^{yz}$ is given by

$$\left|\frac{d\left\langle F^x\right\rangle}{d\lambda}\right| = \left|\langle[F^x, Q^{yz}]\rangle\right|. \tag{S8}$$

The ratio of the measurement variance $(\Delta\lambda)^2$ to the standard quantum limit $(\Delta\lambda_{\mathrm{SQL}})^2$ is thus

$$\xi^2 \equiv \left(\frac{\Delta\lambda}{\Delta\lambda_{\mathrm{SQL}}}\right)^2 = \frac{4f^2N\mathrm{Var}\left(F^x\right)}{\left|\langle[F^x, Q^{yz}]\rangle\right|^2} = \frac{f^2\mathrm{Var}\left(F^x\right)}{C^2N}. \tag{S9}$$

For our atoms with internal spin $f = 1$, Eq. (S9) simplifies to $\xi^2 = \mathrm{Var}\left(F^x\right)/(C^2N)$. The Wineland parameter is related to the normalized variance ζ^2 plotted in the main text as $\xi^2 = \zeta^2/C$, so that the SQL is represented by a line at $\zeta^2 = C$.

III. CALIBRATING CONTRAST AND CONFIRMING LARMOR INVARIANCE

To calculate the normalized variances presented in the main text, we determine the commutator CN from the average populations of the Zeeman states after the readout spin rotation, as described in the Methods (Sec. F). The ability to determine both the noise $\mathrm{Var}\left(F_x\right)$ and the commutator $CN = \left|\langle[F^x, Q^{yz}]\rangle\right|/2$ from the same data set is a feature of the Larmor-invariant spin-1 system and is advantageous for minimizing sensitivity to any drifts in experimental parameters. However, an alternative approach is to determine the contrast C by a separate interferometric measurement, as suggested by the role of the metrological squeezing parameter in quantifying enhanced interferometric sensitivity. Here, we present such a measurement of the contrast C_{Rabi} of a Rabi oscillation on the $\{F_x, Q_{yz}, Q_0\}$ sphere, which corroborates the method used in the main text and confirms the assumption of Larmor invariance.

We determine the contrast C_{Rabi} from the amplitude of a Rabi oscillation after spin-nematic squeezing. For this measurement, we prepare the atoms in $m_F = 0$ before driving the cavity for 50 μs to induce pair-creation dynamics. Up to this point, the sequence is the same as that used for the data in Fig. 2 of the main text. After the dynamics, we apply a spin rotation by an angle $\theta = \Omega_{\mathrm{Raman}}t$ about an axis $F^x\cos\varphi_L + F^y\sin\varphi_L$ in the F^x–F^y plane. Since spin-nematic squeezing dynamics are symmetric under global Larmor rotations (as verified at the end of this section), the choice of Larmor phase φ_L is arbitrary. We thus visualize the spin rotation in Fig. S1a as a Rabi oscillation about F^x on the $\{F^x, Q^{yz}, Q^0\}$ sphere, with oscillation frequency $2\Omega_{\mathrm{Raman}}$.

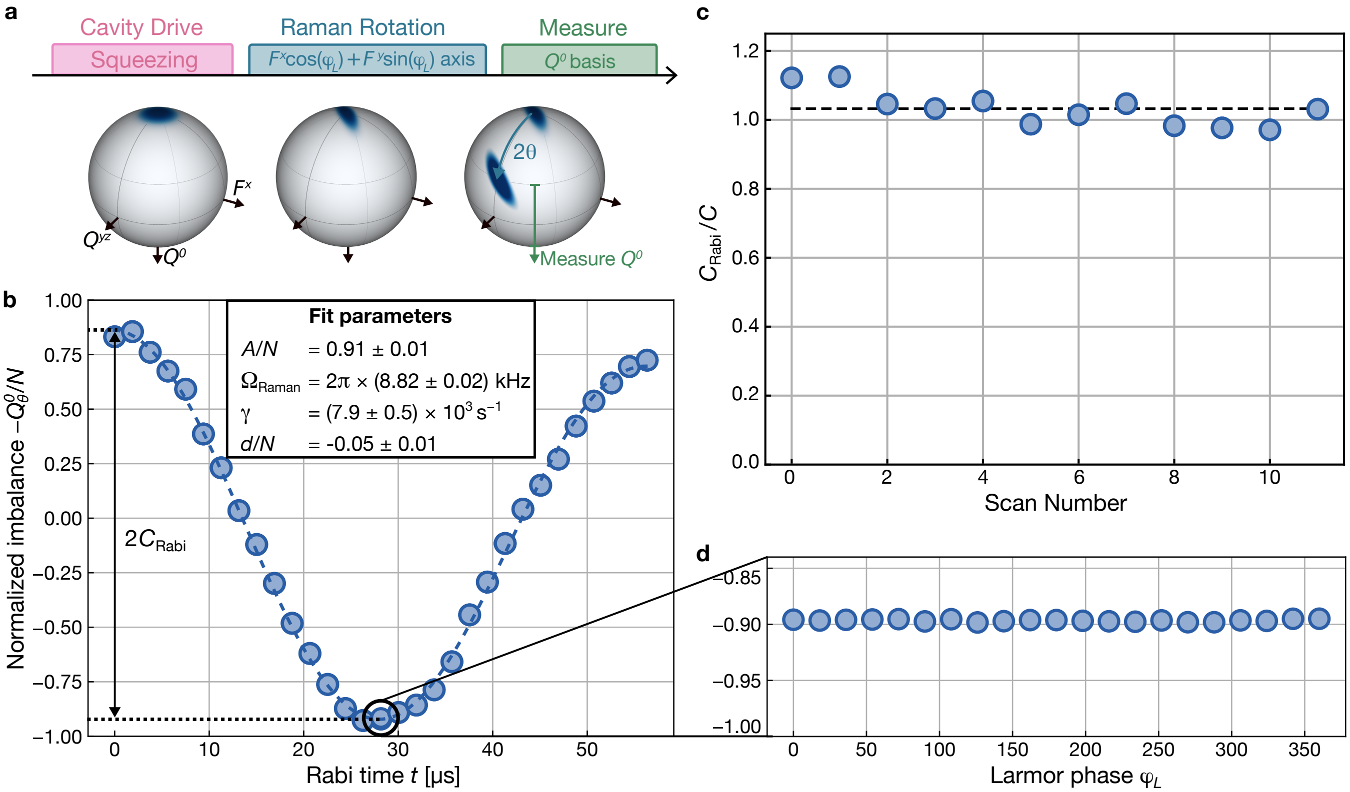

Fig. S1. **Direct measurement of contrast.** **a**, After applying the cavity drive field for 50 μs to generate spin-nematic squeezing, we perform a rotation about an arbitrary axis with Larmor phase φ_L in $F^x - F^y$ plane. When $\varphi_L = 0$ this rotation corresponds to Rabi oscillations that are visualized on the $\{F^x, Q^{yz}, Q^0\}$ sphere. **b**, Following the rotation, we measure the normalized imbalance $-Q^0_\theta/N = (N'_0 - (N'_{+1} + N'_{-1}))/N$ as a function of Rabi oscillation time t. The dashed line is a fit of the model in Eq. (S12). From this fit, we extract the contrast $C_{\text{Rabi}} = \left|Q^0_{\theta=0^\circ} - Q^0_{\theta=90^\circ}\right|/(2N) = 0.89 \pm 0.01$. **c**, We compare the contrast C_{Rabi} to the value $C = (3Q^0_{\theta=90^\circ} - 1)/(2N)$ computed as derived in Methods Sec. F. The percent-level difference indicated by the average ratio $C_{\text{Rabi}}/C = 1.03 \pm 0.01$ (black dashed line) is attributable to the dephasing of the Rabi oscillation at rate γ,which results in conservative estimates of normalized variances and squeezing parameters in the main text. **d**, Measurements of population imbalance after a rotation by $\theta = 90^\circ$ confirm that the calibration of contrast is independent of the choice of Larmor phase φ_L. Data shown are the average over typically 50 iterations.

In Fig. S1b we determine the Rabi oscillation amplitude by evaluating the normalized population imbalance $-Q^0_\theta/N \equiv (N'_0 - (N'_{+1} + N'_{-1}))/N$ as a function of $\theta = \Omega_{\text{Raman}}t$. The full expression for the resulting Rabi oscillation in terms of the initial expectation values $\langle Q^0\rangle$, $\langle Q^{yz}\rangle$, and $\langle D\rangle = \langle Q^{zz} + Q^{yy} - Q^{xx}\rangle/4 + N/3$ is

$$Q^0_\theta = \cos(2\theta)\left\langle Q^0\right\rangle + \sin(2\theta)\left\langle Q^{yz}\right\rangle + (1-\cos(2\theta))\left\langle D\right\rangle. \tag{S10}$$

The final term arises from the fact that $\{F_x, Q_{yz}, Q_0\}$ form an approximate rather than exact SU(2) subspace (see Sec. I). The contrast of the Rabi oscillation can be expressed in terms of the operators prior to the spin rotation as

$$\begin{aligned} C_{\text{Rabi}} &= \frac{1}{2N}\left|Q^0_{\theta=0^\circ} - Q^0_{\theta=90^\circ}\right| \\ &= \frac{1}{2N}\left|2\left\langle Q^0 - D\right\rangle\right| \\ &= \frac{1}{2N}\left|\left\langle [F^x, Q^{yz}]\right\rangle\right|, \end{aligned} \tag{S11}$$

which provides an alternative measurement of the contrast C as defined in the main text.

To extract the contrast C_{Rabi}, we fit measurements of the population imbalance $Q^0(t)$ after a Raman pulse of duration t with a function of the form

$$-Q^0(t) = A\,e^{-(\gamma\,t)^2}\cos(2\Omega_{\text{Raman}}t) + d, \tag{S12}$$

where Ω_{Raman} is the Rabi frequency and γ is the Rabi dephasing rate. The amplitude A and offset d together account for both the final term in Eq. (S10) and incoherent collisional spin-exchange interactions between the readout rotation and imaging, where the latter is dominant in our system. We use the fit to extract the contrast $C_{\mathrm{Rabi}} = \left|Q^0(t = \pi/2\Omega_{\mathrm{Raman}}) - Q^0(t = 0)\right|/(2N) = 0.89(1)$.

The primary source of imperfect contrast is spin-changing collisions that occur in the time (20 ms) between the Raman rotation and the fluorescence readout. These collisions permit states polarized with either all atoms in $m = 0$ or all atoms in $m = \pm 1$ to decay into a mixture of all three states. This process reduces contrast and introduces an offset to the Rabi oscillation, but does not directly affect the measurement of $\mathrm{Var}\,(F^x)$, since the collisions preserve the population difference $N'_{+1} - N'_{-1}$ from which we infer the polarization F^x in the experiment. Additionally, dephasing from inhomogeneity in the Raman rotation and detuning due to a finite ratio $\Omega_{\mathrm{Raman}}/q$ reduce the measured value of $\left|Q^0_{\theta=90^\circ}\right|$. The measurement of contrast C used for evaluating normalized variances depends only on $Q^0_{\theta=90^\circ}$ and not on $Q^0_{\theta=0^\circ}$, and is thus more strongly impacted by these effects, leading to a 3% difference between the two measurements as shown in Fig. S1c. This difference indicates that the normalized variances and squeezing parameters reported in the main text are conservative estimates.

In the main text, we rely on the Larmor invariance of the states generated by spin-nematic squeezing to extract the contrast C from the same data as the variance of F^x. In particular, the Raman pulse used to convert F^x to F^z converts Q^{xx} to Q^{zz}, and we assume the equality $\langle Q^{yy}\rangle = \langle Q^{xx}\rangle$ in determining the contrast (Methods Sec. F). Directly measuring $\langle Q^{yy}\rangle$ requires shifting the phase φ_L of the Raman pulse by 90°. We verify the equality $\langle Q^{yy}\rangle = \langle Q^{xx}\rangle$ by varying the phase φ_L of the Raman pulse in the sequence of Fig. S1a with $\theta = \pi/2$, i.e., in the same sequence used for characterizing global squeezing in the main text. To controllably vary the Larmor phase, we adjust the start time of the Raman pulse by a variable delay $\Delta t \leq 2\pi/\omega_z$, where ω_z is the Larmor frequency, while keeping the waveform of the synthesized pulse fixed. We have verified that this procedure produces a Ramsey fringe as a function of $\varphi_L = \omega_z \Delta t$ when applied to a spin-polarized state that is initialized along F_x by a prior Raman pulse. When instead the state is initialized by spin-nematic squeezing, the measurement result is independent of φ_L, as seen in Fig. S1d. The measured mean values $Q^0_{\theta=90^\circ}(\varphi_L = 0^\circ) = \langle Q^{yy}\rangle + N/3$ and $Q^0_{\theta=90^\circ}(\varphi_L = 90^\circ) = \langle Q^{xx}\rangle + N/3$ are equal to within 0.1%, directly confirming the assumption $\langle Q^{xx}\rangle = \langle Q^{yy}\rangle$ used to determine the contrast C.

IV. SQUEEZING DYNAMICS

We present a theoretical formulation of the spin-nematic squeezing dynamics. This model provides a basis to estimate the contributions of technical noise in our measured squeezing, as well as the effects of cavity dissipation. Finally, we discuss fundamental limits set by the cavity cooperativity on the degree of multimode squeezing attainable in our protocol for preparing graph states.

A. Equations of Motion

We analyze the dynamics of spin-nematic squeezing for a system initialized with all atoms in $m = 0$, focusing on the experimentally relevant regime of early times where the population in states $m = \pm 1$ remains small ($N_{+1} + N_{-1} \ll N$). To allow for effects of finite atomic temperature, we begin by writing down a Hamiltonian that incorporates non-uniform coupling to the cavity mode,

$$H = \frac{\chi}{2N}\left(\mathcal{F}^x\mathcal{F}^x + \mathcal{F}^y\mathcal{F}^y\right) + \frac{q}{2}Q^0. \tag{S13}$$

Here the collective spin $\mathbf{F}$ defined in the main text is replaced with a weighted collective spin $\boldsymbol{\mathcal{F}} = \sum_i w_i f_i$, which includes a correction for inhomogeneous cavity couplings $w_i \propto \Omega_i$, where Ω_i denotes the ac Stark shift per intracavity photon experienced by the i^{th} atom. The weights w_i are normalized such that $\langle w_i\rangle = 1$.

We describe the early-time dynamics in the two dimensional subspace spanned by the weighted spin operators $\mathcal{F}^x$ and $\mathcal{Q}^{yz}$. During these early times, commutators relevant to the dynamics are $[\mathcal{F}^x, \mathcal{F}^y] = 2i\sum_i w_i^2 f_i^z \approx 0$, $[\mathcal{F}^x, Q^{yz}] \approx -2iN$, and $[Q^0, \mathcal{F}^x] = 2i\mathcal{Q}^{yz}$. The Heisenberg equations $d\mathcal{O}/dt = i[H, \mathcal{O}]$ for both spin observables in this space are

$$\frac{d}{dt}\begin{bmatrix}\mathcal{F}^x\\ \mathcal{Q}^{yz}\end{bmatrix} = \begin{bmatrix}0 & -q\\ q+2\chi & 0\end{bmatrix}\begin{bmatrix}\mathcal{F}^x\\ \mathcal{Q}^{yz}\end{bmatrix}. \tag{S14}$$

Identical dynamics occur in the subspace spanned by $\mathcal{F}^y$ and $\mathcal{Q}^{xz}$ so that state remains invariant under global spin rotations about F^z.

The linear equations of motion for $\mathcal{F}^x$ and $\mathcal{Q}^{yz}$ can be solved exactly. This system has eigenvalues $\pm\lambda$ where $\lambda = \sqrt{-q(q+2\chi)}$. The corresponding solutions are

$$\begin{aligned}\mathcal{F}_{+\lambda}(t) &= \frac{e^{\lambda t}}{\sqrt{1+(\lambda/q)^2}}\left(\mathcal{F}^x(0) - \frac{\lambda}{q}\mathcal{Q}^{yz}(0)\right)\\ \mathcal{F}_{-\lambda}(t) &= \frac{e^{-\lambda t}}{\sqrt{1+(\lambda/q)^2}}\left(\mathcal{F}^x(0) + \frac{\lambda}{q}\mathcal{Q}^{yz}(0)\right).\end{aligned} \tag{S15}$$

In general, these two operators are not orthogonal unless $\chi = -q$. The expectation value and variance of any observable $\mathcal{F}_\phi = \cos\phi\,\mathcal{F}^x - \sin\phi\,\mathcal{Q}^{yz}$ can be calculated from these operators by noting that $\mathcal{F}_\phi(t) = a\mathcal{F}_{-\lambda}(t) + b\mathcal{F}_{+\lambda}(t)$ where a and b are real coefficients that are independent of time and may be solved for from the expressions at time $t = 0$. The variance for a particular spinor angle ϕ at time t is then given by

$$\left\langle \mathcal{F}_\phi(t)^2\right\rangle = e^{-2\lambda t}a^2\left\langle \mathcal{F}_{-\lambda}(0)^2\right\rangle + ab\left\langle\{\mathcal{F}_{+\lambda}(0), \mathcal{F}_{-\lambda}(0)\}\right\rangle + e^{2\lambda t}b^2\left\langle \mathcal{F}_{+\lambda}(0)^2\right\rangle, \tag{S16}$$

where the cross term proportional to ab again highlights that $\mathcal{F}_{-\lambda}(t)$ and $\mathcal{F}_{+\lambda}(t)$ are in general not orthogonal. At $t = 0$ the system is in a coherent state with variance $\left\langle \mathcal{F}_\phi(0)^2\right\rangle = N$ at the level of projection-noise for all values of ϕ. This condition yields the constraint

$$a^2 + b^2 + 2ab\frac{1-(\lambda/q)^2}{1+(\lambda/q)^2} = 1, \tag{S17}$$

which reduces to $a^2 + b^2 = 1$ when $\chi = -q$.

The operator with maximal variance (the anti-squeezed quadrature) for $t \gtrsim 1/\lambda$ is determined by maximizing the coefficient b of the exponentially growing mode (see Eq. (S16)) subject to the constraint of Eq. (S17). This is achieved when $b = -\chi/\lambda$ and $a = -(\chi+q)/\lambda$, corresponding to an anti-squeezing $\zeta^2_{\text{max}} = |\chi/\lambda|^2\ e^{2\lambda t}$ at an angle $\phi = \arctan(\lambda/q)$. Since the dynamics preserve phase space area, this corresponds to a minimum variance $\zeta^2_{\text{min}} = 1/\zeta^2_{\text{max}}$ at an angle $\phi_{\text{min}} = \arctan(-q/\lambda)$.

B. Technical Limitations on Squeezing

The model of the dynamics in Sec. IV A provides a foundation for estimating the effect of experimental noise on the amount of observed squeezing. Two primary limits are fluctuations in the collective interaction strength χ and inhomogeneous coupling of the thermal distribution of atoms to the cavity, where the latter effect introduces a slight discrepancy between the collective mode squeezed by the cavity and the observable detected in fluorescence imaging.

1. *Fluctuations in Interaction Strength*

The collective interaction strength χ varies the angle of squeezing as $\phi_{\text{min}} = \arctan(-q/\lambda)$, and so fluctuations in χ act to wash out the squeezing. We can write the variance as a function of spinor phase as

$$\zeta^2(\phi) = \zeta^2_{\text{min}} + \sin^2(\phi - \phi_{\text{min}})\left(\zeta^2_{\text{max}} - \zeta^2_{\text{min}}\right). \tag{S18}$$

To find the effect of fluctuations $\Delta\chi$ in interaction strength, we expand Eq. (S18) around the angle ϕ_{min} of optimum squeezing and write our expression in terms of χ. To leading order in $\Delta\chi$, we are left with the additional noise $\Delta\zeta^2_{\text{interaction}}$ from interaction strength fluctuations, which is given by

$$\Delta\zeta^2_{\text{interaction}} = \zeta^2_{\text{meas}} - \zeta^2_{\text{min}} = \zeta^2_{\text{max}}\frac{q}{2|q+2\chi|}\left(\frac{\Delta\chi}{\chi}\right)^2. \tag{S19}$$

This is a lower bound on the added noise, since the angle ϕ_{min} at finite times has larger fluctuations than in the $t > \lambda^{-1}$ limit. In principle, added noise from interaction strength fluctuations can be suppressed by working in the regime of $\chi \gg q$. However, we do not operate in this limit because setting $\chi \sim q$ maximizes the squeezing rate λ relative to the fundamental cavity dissipation, as we shall see in Sec. IV C.

The fluctuations in interaction strength χ in our experiment arise from variations in the number of intracavity photons $\overline{n}$, the number of coupled atoms N, or the detunings from the two virtual Raman processes $\delta_\pm$ (see Eq. (8)). These sources of noise are correlated, as the number of intracavity photons

$$\overline{n} = \overline{n_i}\frac{(\kappa/2)^2}{\delta_c^2 + (\kappa/2)^2} \tag{S20}$$

not only depends on the input drive strength $\overline{n_i}$, but also depends on the detuning from cavity resonance. The detunings δ_c and $\delta_\pm$ in turn depend on the atom number N due to the dispersive shift $\delta_N = 4\Omega N$ of the cavity resonance induced by the atoms. The two direct sources of fluctuations in χ are then the number of input photons $\overline{n_i}$ and the atom number N, which lead to total fluctuations

$$\left(\frac{\Delta\chi}{\chi}\right)^2 = \left(\frac{\Delta\overline{n_i}}{\overline{n_i}}\right)^2 + \alpha^2\left(\frac{\Delta N}{N}\right)^2, \tag{S21}$$

where

$$\alpha = 1 + \left|\frac{2\delta_N}{\delta_c}\right| + \left|\frac{\delta_N}{\delta_-}\right| \tag{S22}$$

evaluates to $\alpha \approx 2$ for our parameters. We stabilize the drive input power to ensure $\Delta\overline{n_i}/\overline{n_i} < 5\%$, and we reduce fluctuations in atom number by post-selecting so that $\Delta N/N < 5\%$ within each data set. At $\Delta\chi/\chi < 10\%$, and a typical value of $\zeta^2_{\text{max}} = 10$, using the values from Methods Sec. C, the additional noise from interaction strength fluctuations is $\Delta\zeta^2_{\text{interaction}} \approx 0.02$.

2. *Inhomogeneous Atom-Cavity Coupling*

Our fluorescence imaging measures a uniformly weighted collective spin F^x, while the cavity couples to the inhomogeneously weighted collective spin $\mathcal{F}^x$ defined in Sec. IV A. Any width in the distribution of coupling weights w_i manifests itself in reduced squeezing. Without loss of generality, we assume $\mathcal{F}^x$ is the squeezed observable and compute the projection of the measured observable on the squeezed observable: $\text{Tr}(F^x\mathcal{F}^x)/(|\mathcal{F}^x||F^x|) = \langle w_i\rangle/\sqrt{\langle w_i^2\rangle}$. The excess noise is given by the magnitude of the remaining component,

$$\Delta\zeta^2_{\text{coupling}} = 1 - \frac{\langle w_i\rangle^2}{\langle w_i^2\rangle} = \frac{\text{Var}\,(w_i)}{\text{Var}\,(w_i) + \langle w_i\rangle^2}. \tag{S23}$$

The variance in couplings comes primarily from the thermal distribution of the atomic states. We parameterize the temperature by the ratio $\beta = U_0/(k_B T)$ of the lattice depth to the atomic temperature. Assuming a harmonic trap, the excess noise Eq. (S23) for a single lattice site is given by

$$\Delta\zeta^2_{\text{coupling}} = 1 - \frac{2\beta(4+\beta)}{(\beta+2)^2\left(\exp\left(8\beta^{-1}\right) - 2\exp\left(4\beta^{-1}\right) + 3\right)}. \tag{S24}$$

In the low temperature limit $\beta \to \infty$, to leading order the added noise is

$$\Delta\zeta^2_{\text{coupling}} = 12\beta^{-2}. \tag{S25}$$

For an ensemble near cavity center with an inverse temperature of $\beta = 15$, Eq. (S24) limits squeezing to $\zeta^2 > 0.08$.

We directly measure the distribution of couplings w_i via microwave spectroscopy, probing the ac Stark shift induced by the drive field on the hyperfine clock transition $|f = 1, m_f = 0\rangle \to |2, 0\rangle$. The drive light, detuned from atomic resonance by $\Delta = -2\pi \times 9.5$ GHz, induces a differential ac Stark shift that is directly proportional to the weight w_i for each atom. We measure the distribution of Stark shifts at different drive intensities, as shown in Fig. S2. The measured spectra are well fit by a model of a thermal distribution with inverse temperature $\beta = 15$, exhibiting variances and means that directly corroborate the bound established in Eqs. (S23)-(S24).

C. Cavity Dissipation

The unitary dynamics described in Sec. IV A are modified by decay channels inherent to any real cavity system. As described in Methods Sec. C and Refs. [6, 7], spin-exchange interactions in the cavity are mediated by a virtual

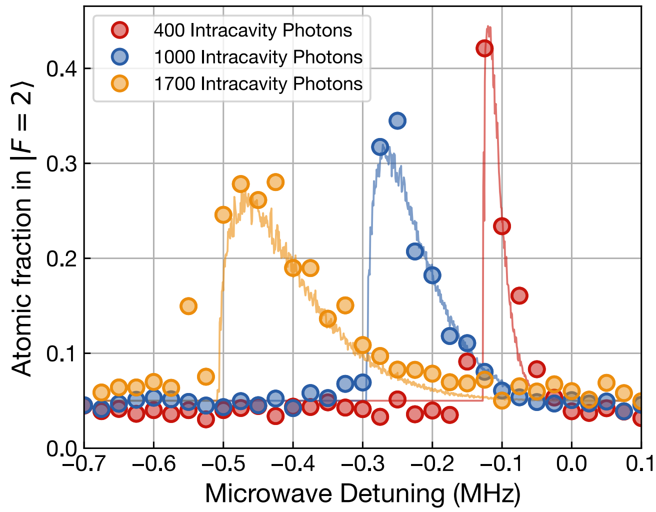

Fig. S2. Measurement of the drive-induced ac Stark shift on the $|f=1, m_f=0\rangle \to |2,0\rangle$ transition. Red, blue, and gold indicate increasing intracavity photon number. The measured distributions of Stark shifts (circles) are well described by a numerical fit based on a thermal distribution of atomic positions with a ratio $\beta = 15$ of trap depth to temperature.

process in which atoms collectively scatter photons from a vertically polarized drive field into a horizontally polarized cavity mode. For coherent interactions, these horizontally polarized photons are subsequently scattered back into the vertical drive mode, allowing for unitary transfer of information among the atoms. However, in practice, photons may also be lost before completing the unitary dynamics and thereby carry away quantum information.

A photon may be lost either due to the finite cavity lifetime or by atomic scattering into free space. In the case of cavity decay, the loss of a photon is accompanied by creation or annihilation of a collective spin excitation. This decay channel is described by the Lindblad operators $L_\pm = \sqrt{\gamma_\pm}\mathcal{F}^\pm$ and has a characteristic strength $\Gamma_{\mathrm{coll}} = 2N(\gamma_+ + \gamma_-)$ that, in analogy to the collective interaction strength χ, is enhanced by the number of atoms. The ratio of the collective decay to the collective interaction strength

$$\frac{\Gamma_{\mathrm{coll}}}{\chi} = \frac{\kappa}{\delta_-} \tag{S26}$$

is determined by the detuning δ_- from the dominant Raman process in our experiment.

To quantify the impact of the collective decay process on the squeezing, we write down the Lindblad equation of motion for the squeezed quadrature $\mathcal{F}_{-\lambda}$,

$$\frac{d\left\langle \mathcal{F}_{-\lambda}^2\right\rangle}{dt} = \left\langle i[H, \mathcal{F}_{-\lambda}^2] + \sum_r 1/2\left(L_r^\dagger[\mathcal{F}_{-\lambda}^2, L_r] + [L_r^\dagger, \mathcal{F}_{-\lambda}^2]L_r\right)\right\rangle, \tag{S27}$$

with the two loss operators $L_\pm = \sqrt{\gamma_\pm}\mathcal{F}^\pm$. Under the simplifying assumptions of uniform couplings ($\mathcal{F}^\pm = F^\pm$), $\chi \approx -q$ and sufficiently early-time dynamics, the equation of motion for squeezing is

$$\frac{d\left\langle \mathcal{F}_{-\lambda}^2\right\rangle}{dt} = -2\lambda\left\langle \mathcal{F}_{-\lambda}^2\right\rangle + N\Gamma_{\mathrm{coll}}. \tag{S28}$$

The steady state of this equation leads to a bound on the variance due to collective decay of

$$\Delta\zeta_{\mathrm{coll}}^2 = \left\langle \mathcal{F}_{-\lambda}^2\right\rangle/N \geq \Gamma_{\mathrm{coll}}/(2\lambda). \tag{S29}$$

The variance exponentially decays to this bound at a rate proportional to $\exp(-2\lambda)$. At finite times, the effect of the bound is mathematically equivalent to mixing the ideal squeezed state achieved under unitary dynamics with vacuum fluctuations on a beam splitter with transmission $1 - \Delta\zeta_{\mathrm{coll}}^2$.

Additionally, photons may be lost due to free-space scattering at a rate Γ_{sc} per atom. Free-space scattering is not a collective process, as the scattered photons carry away information about individual atoms. On cavity resonance, free-space scattering is thus suppressed with respect to interactions by a factor $N\eta/k$, where $N\eta$ is the collective cooperativity for a cycling transition and the numerical factor $k = 96$ includes the strengths of the atomic transitions in our level scheme [7]. Overall, the rate of free-space scattering in the limit $\delta_- > \kappa$ is then

$$\frac{\Gamma_{\mathrm{sc}}}{\chi} = \frac{96}{N\eta}\frac{\delta_-}{\kappa}. \tag{S30}$$

The effect of a scattering event is to erase correlations between the atom that scatters a photon and the remaining atoms. This erasure of correlations adds noise to the squeezed quadrature at a rate

$$\frac{d\left\langle \mathcal{F}_{-\lambda}^2\right\rangle}{dt} = \alpha N \Gamma_{\mathrm{sc}}, \tag{S31}$$

where $\alpha = 2$ for the worst case where an atom is projected into the $m = 0$ state. However, while collective decay only impacts the mode coupled to the cavity, free-space scattering continues to impact all modes that have already been squeezed. On average each mode is impacted by scattering for a total duration $\tau \times M/2$, where τ is the duration of each squeezing pulse, yielding a noise contribution

$$\Delta\zeta_{\mathrm{sc}}^2 = M\tau\Gamma_{\mathrm{sc}}. \tag{S32}$$

While free-space scattering additionally reduces the contrast by a factor of approximately $e^{-M\tau\Gamma_{\mathrm{sc}}/2}$, in the regime of strong squeezing the added noise is the dominant limitation.

The impact of the two noise contributions $\Delta\zeta_{\mathrm{coll}}^2$ and $\Delta\zeta_{\mathrm{sc}}^2$ can be minimized by choosing optimal values of the interaction strength χ and detuning δ_-. An interaction strength of $\chi = -q$ optimizes the speed of the coherent dynamics λ/χ. Optimizing the two limits for the mode with maximal scattering, with $\tau\lambda = 1$, yields a detuning of $\delta_- = \kappa\sqrt{N\eta/(192M)}$, balancing the impact of the two loss channels to minimize their combined effect. In practice, we experimentally optimize squeezing, which takes into account additional noise sources, resulting in a slight deviation from the theoretical optimum.

Having derived expressions for both collective decay and free-space scattering, we summarize the impact on the experiments in the current work in Sec. IV D and derive fundamental limits on the scaling of the squeezing in Sec. IV E.

D. Summary of Noise Contributions

We summarize the impact of all noise processes limiting our squeezing in Table S1. The effects of cavity decay, free-space scattering, and coupling variation are all mathematically equivalent to mixing the squeezed quantum state with zero point fluctuations, as if on a beam splitter. Starting from the minimal possible variance given unitary dynamics, $1/\zeta_{\mathrm{max}}^2$, each process results in a factor of $(1 - \Delta\zeta_i^2)$ reduction in the amount by which the state is squeezed. We calculate the combined effect of these noise sources $\Delta\zeta_i^2$, assuming that they are all independent, as

$$\Delta\zeta_{\mathrm{total}}^2 = 1 - \Pi_i(1 - \Delta\zeta_i^2). \tag{S33}$$

Photon shot noise and interaction strength noise behave differently, since they directly add noise rather than degrading the state toward the standard quantum limit. These terms are added at the end using standard propagation of uncertainty. Finally, we divide by the Rabi oscillation contrast $C_{\mathrm{Rabi}} = 0.89$ measured in Sec. III to obtain the expected normalized variance ζ^2.

In principle, working at larger atom number increases the collective cooperativity, decreasing the relative effects of cavity dissipation. However, in addition to the noise sources in Table S1, different collective modes are sensitive to technical noise in the readout procedure, as discussed in Sec. E. The example data presented in Table S1 are measured in the $\uparrow\downarrow\uparrow\downarrow$ mode, which has negligible technical noise (see Extended Data Fig. 1). For Figs. 2 and 3 of the main text we squeeze up to two collective modes, and these modes can always be mapped to the two collective modes with minimal technical noise using local Larmor rotations. In this case we choose an atom number of $N = 1.5 \times 10^4$, which is limited by the density of atoms in the trap, as any collisional spin exchange interactions are incoherent with the photon-mediated interactions, reducing the effective spin length. For the square graph state all 4 collective modes need to be squeezed, and the technical noise in our projection noise calibration becomes a relevant parameter, so we reduce the atom number in Fig. 4 of the main text to $N = 8 \times 10^3$.

E. Fundamental Scaling

Fundamental limits to the degree of squeezing attainable by global cavity-mediated interactions among N atoms are governed by the collective cooperativity $N\eta$ [8], where $\eta = 4g^2/(\kappa\Gamma)$ is the single-atom cooperativity. In this

	Figs. 2 and 3	Fig. 4
δ_-	$-2\pi \times 1.3$ MHz	$-2\pi \times 1.6$ MHz
N	1.5×10^4	8×10^3
χ	$-2\pi \times 4.3$ kHz	$-2\pi \times 1.5$ kHz
λ	$2\pi \times 3.0$ kHz	$2\pi \times 1.4$ kHz
τ	50 μs	100 μs
$1/\zeta^2_{\max}$	0.13	0.28
Photon shot noise	0.05	0.05
Coupling variation	0.08	0.08
Interaction strength noise	0.02	0.02
Cavity photon loss	0.14	0.07
Free space scattering	0.02	0.07
Measured contrast C_{Rabi}	0.89	0.89
Expected ζ^2	0.44	0.56
Observed ζ^2	0.52 ± 0.07	0.56 ± 0.09

Table S1. Summary of noise sources contributing to the variances in Figs. 2 and 3 of the main text, along with the relevant experimental parameters from Extended Data Table 1. The method of calculating the expected variance from the individual noise contributions is described in Sec. IV D.

section, we derive limits on squeezing multiple collective modes which demonstrate the scalability of our graph-state preparation protocol. We focus first on the specific case of the spin-nematic squeezing employed in this work, and additionally comment on generalizations to other methods of cavity-mediated spin squeezing.

The fundamental limit on squeezing set by the cavity cooperativity arises from two dissipation processes: loss of photons from the cavity mode that mediates interactions; and scattering of photons into free space. These loss processes are parameterized by the rates Γ_{coll} and Γ_{sc} in Eq. (S30). The effect of the free-space scattering is proportional to the number of modes M because scattering at any point during the protocol can reduce squeezing. Conversely, collective decay does not depend on M because it acts only on the collective mode coupled to the cavity. To place free-space scattering and cavity loss on an even footing, we imagine dividing the squeezing of each collective mode into multiple segments interleaved with squeezing of the other collective modes, so that the scattering is interspersed with the coherent dynamics. Any scattering loss while addressing each of the M modes should then be included as a component of Eq. (S28). The full equation of motion for the variance of each collective mode is thus

$$\frac{d\zeta^2_{\mathrm{min}}}{dt} = -2\lambda\zeta^2_{\mathrm{min}} + \Gamma_{\mathrm{coll}} + 2M\Gamma_{\mathrm{sc}}. \tag{S34}$$

The squeezing is optimized by choosing the drive-cavity detuning that minimizes the total contribution to Eq. (S34) from scattering and cavity decay:

$$\left(\frac{\delta_-}{\kappa}\right)^2 = \frac{1}{192}\frac{N\eta}{M}. \tag{S35}$$

This optimum detuning is set by the collective cooperativity per mode $N\eta/M$ and leads to an overall variance

$$\zeta^2_{\mathrm{min}} = 8\left(\frac{N\eta}{3M}\right)^{-1/2}. \tag{S36}$$

While these derivations focus on variance ζ^2, the same scaling applies to the Wineland squeezing parameter ξ^2.

Equation (S36) shows that our protocol for generating arbitrary M-node graph states by squeezing M collective modes yields fixed squeezing at constant atom number per ensemble (N/M), independent of the number of graph nodes. The protocol requires order M squeezed modes and order M sets of rotations. However, at fixed atom number per ensemble, with increasing M the increased collective interaction strength causes each mode to be squeezed faster, so that the total interaction time remains fixed. The protocol can thus be scaled to larger arrays of ensembles, limited only by the spatial extent of the cavity mode and the fidelity of local addressing.

In practice, scaling to larger numbers of ensembles requires addressing technical noise sources that scale with the total atom number. Fractional imaging noise needs to be smaller than atom projection noise in order to observe squeezing. Thus, technical noise must be reduced in proportion to the lower standard quantum limit for the larger numbers of atoms. Additionally, free-space scattering can change the internal state of atoms from the $f = 1$ to the $f = 2$ manifold and thereby shift the cavity resonance away from the optimal detuning, an effect that increases with higher atom number. The effect can be mitigated by squeezing on a cycling transition [9, 10] or, in our present squeezing scheme, by increasing the atom-cavity detuning Δ or actively stabilizing the drive-cavity detuning δ.

The limit on squeezing $\xi^2 \propto 1/\sqrt{(N/M)\eta}$ set by the collective cooperativity per mode generalizes to a wide variety of methods of cavity spin squeezing, including approaches employing either photon-mediated interactions [8, 11] or quantum non-demolition measurements [12]. Improvements to both the numerical prefactor and the overall scaling with cooperativity are possible, however, by a suitable choice of atomic level scheme. Notably, for squeezing on a cycling transition, the scaling for the single-mode case improves to $\xi^2 \propto 1/(N\eta)$ [9, 10]. Optimizing the scheme for the collective entangling operations may facilitate future work seeking the error-correction threshold of $-10\log\xi^2 = 20.5$ dB [13], or generating discrete-variable graph states in arrays of single atoms.

[1] D. J. Wineland, J. J. Bollinger, W. M. Itano & D. Heinzen. Squeezed atomic states and projection noise in spectroscopy. *Physical Review A* **50**, 67 (1994).

[2] L. Pezze, A. Smerzi, M. K. Oberthaler, R. Schmied & P. Treutlein. Quantum metrology with nonclassical states of atomic ensembles. *Reviews of Modern Physics* **90**, 035005 (2018).

[3] Y.-Q. Zou, L.-N. Wu, Q. Liu, X.-Y. Luo, S.-F. Guo, J.-H. Cao, M. K. Tey & L. You. Beating the classical precision limit with spin-1 Dicke states of more than 10,000 atoms. *Proceedings of the National Academy of Sciences* **115**, 6381–6385 (2018). Also see Materials and Methods.

[4] S. L. Braunstein & C. M. Caves. Statistical distance and the geometry of quantum states. *Phys. Rev. Lett.* **72**, 3439–3443 (1994).

[5] V. Giovannetti, S. Lloyd & L. Maccone. Advances in quantum metrology. *Nature Photonics* **5**, 222–229 (2011).

[6] E. J. Davis, G. Bentsen, L. Homeier, T. Li & M. H. Schleier-Smith. Photon-mediated spin-exchange dynamics of spin-1 atoms. *Physical Review Letters* **122**, 010405 (2019).

[7] A. Periwal, E. S. Cooper, P. Kunkel, J. F. Wienand, E. J. Davis & M. Schleier-Smith. Programmable interactions and emergent geometry in an array of atom clouds. *Nature* **600**, 630–635 (2021).

[8] A. S. Sørensen & K. Mølmer. Entangling atoms in bad cavities. *Physical Review A* **66**, 022314 (2002).

[9] G. P. Greve, C. Luo, B. Wu & J. K. Thompson. Entanglement-enhanced matter-wave interferometry in a high-finesse cavity. *Nature* **610**, 472–477 (2022).

[10] J. G. Bohnet, K. C. Cox, M. A. Norcia, J. M. Weiner, Z. Chen & J. K. Thompson. Reduced spin measurement back-action for a phase sensitivity ten times beyond the standard quantum limit. *Nature Photonics* **8**, 731–736 (2014).

[11] I. D. Leroux, M. H. Schleier-Smith & V. Vuletić. Implementation of cavity squeezing of a collective atomic spin. *Physical Review Letters* **104**, 073602 (2010).

[12] O. Hosten, N. J. Engelsen, R. Krishnakumar & M. A. Kasevich. Measurement noise 100 times lower than the quantum-projection limit using entangled atoms. *Nature* **529**, 505–508 (2016).

[13] N. C. Menicucci. Fault-tolerant measurement-based quantum computing with continuous-variable cluster states. *Physical Review Letters* **112**, 120504 (2014).